PAPER

Check for updates

A transparent, ultrastretchable and fully recyclable gelatin organohydrogel based electronic sensor with broad operating temperature†

Zhihui Qin,[a] Xia Sun,[a] Haitao Zhang,[a] Qingyu Yu,[a] Xueyuan Wang,[a] Shaoshuai He,[a] Fanglian Yao [ID] *[abc] and Junjie Li [ID] *[ac]

Flexible and stretchable electronics have received tremendous attention for next-generation human-friendly electronic applications. However, fabrication of transparent, fully recyclable and stretchable electronic sensors with low-temperature stability using biocompatible natural polymer-based hydrogels still remains a great challenge. In this study, a green and fully recyclable stretchable electronic sensor with high transparency and ultra-low operating temperature is constructed using ionic conductive gelatin organohydrogels. These gelatin organohydrogels are prepared by a simple strategy of immersing gelatin pre-hydrogels in citrate (Na_3Cit) water/glycerol solutions. The existence of Na_3Cit in the organohydrogel not only induces the formation of multiple non-covalent cross-linking points, endowing the organohydrogel with high mechanical performances, but also makes the organohydrogel have excellent ionic conductivity. The organohydrogel is also highly transparent and exhibits outstanding antifreezing properties. The mechanical robustness, conductivity and transparency of the organohydrogel can be well maintained even at −60 °C. As a result, a stretchable and transparent electronic sensor based on this organohydrogel is fabricated, which is strain-sensitive with a large linear sensing window and excellent stability. More importantly, the organohydrogel-based electronic sensor can be fully recycled due to the reversible non-covalently crosslinked structure, and the recycled organohydrogel regains its mechanical and sensing properties. The obtained sensors could precisely detect various human activities even below −30 °C, indicating the potential applications of the organohydrogel-based electronic sensor in flexible and stretchable electronics in a broad range of temperature.

1. Introduction

Flexible and stretchable electronics, which allow mechanical deformations of electronic devices without compromising functionalities during their operation, have tremendous applications in various fields (energy storage devices, implantable medical devices, artificial intelligence, wearable electronics, *etc.*).[1–9] Stretchable sensors are the key building units for flexible and stretchable electronics,[10] which need the materials for fabrication of electronic sensors to have appropriate electrical and mechanical properties. Recently, efforts to create soft and stretchable electronic sensors have largely focused on conductive hydrogels due to their good electrical conductivity and flexibility.[11–17] Conductive hydrogels typically used for these sensors are fabricated by embedding carbon nanomaterials (carbon nanotubes and graphene) or intrinsically conductive polymers into traditional hydrogel matrices.[18–20] The easy aggregation properties of these conducting components in the polymer network make these kinds of conductive hydrogels have insufficient mechanical properties and compromised conductivity.[18] In addition, this type of conductive hydrogel is usually black and the transparency of the hydrogel is greatly reduced.[21] These limitations greatly prohibit the use of stretchable electronics in applications such as skin-like sensors and wearable devices. More importantly, the mechanical flexibility of the traditional conductive hydrogel-based electronic sensors will vanish at subzero temperatures due to the formation of ice crystals, further limiting their applications in low-temperature environments.[22]

Integrating excellent mechanical properties, good transparency and broad extreme-temperature tolerance into stretchable electronic sensors is greatly important for practical applications. The excellent mechanical performances can

aSchool of Chemical Engineering and Technology, Tianjin University, Tianjin 300350, China. E-mail: yaofanglian@tju.edu.cn; li41308@tju.edu.cn

bSchool of Materials Science and Engineering, East China Jiaotong University, Nanchang 330013, China

cKey Laboratory of Systems Bioengineering of Ministry of Education, Tianjin University, Tianjin 300350, China

† Electronic supplementary information (ESI) available. See DOI: 10.1039/c9ta13196e

This journal is © The Royal Society of Chemistry 2020

J. Mater. Chem. A, 2020, **8**, 4447–4456 | **4447**

ensure the mechanical matching with dynamic surfaces (such as human skin) and accommodate strain during repeated movements.[23] A good transparency allows visualization of the internal conditions of the electronic devices and reduces the visible difference from human skin.[24] Moreover, the wide extreme-temperature tolerance will broaden their application environments and seasons, even at ultra-low temperature.[25] Benefiting from some unique properties such as good stretchability, high transparency and excellent ionic conductivity, there has been exciting progress in the development of ionic conductive hydrogel-based stretchable electronic sensors.[11,26–28] For example, Kim *et al.* reported a highly stretchable and transparent ionic touch panel using ionically conductive polyacrylamide (PAAm) hydrogels.[27] This hydrogel-based ionic touch panel exhibited precise and fast touch-sensing, even in a highly stretched state. Sui *et al.* developed a highly stretchable and transparent ionic DN hydrogel-based strain sensor with high sensitivity and broad sensing range of strains, which was promising for a new generation of e-skins.[28] Although promising, these hydrogel-based electronic sensors would not operate at subzero temperatures due to freezing of the hydrogels. Recently, although several anti-freezing gels have been constructed by introducing organic agents or highly concentrated salts to be used as electronic sensors,[29–33] all these hydrogel-based sensors are made from synthetic components, which can cause hazards to the human body and environment when used for a long time. Although natural biopolymers, such as alginate, cellulose, hyaluronic acid, collagen, and silk, have been used to develop stretchable and green electronic sensors due to their excellent biocompatibility and controllable biodegradability,[8,34,35] these existing natural polymer-based hydrogels have at least one of several limitations: suffer from poor conductivity, or low extensibility, or low environmental stability (freezing at subzero temperatures), greatly limiting their utility as substrates for stretchable electronic sensors.[36–38] To date, eco-friendly and green electronic sensors with excellent mechanical performances and ultra-low operating temperature have been rarely reported.

Another challenging issue for stretchable electronic sensors is the inability to be recycled upon breakage of the electronic device. Massive electronic waste is produced worldwide.[39] On the one hand, this electronic waste has a huge impact on the environment and cause serious harm to valuable natural resources. On the other hand, single-use electronic items will increase the manufacturing cost and relevant expenditure of consumers. The recyclability of electronics can perfectly solve these problems. Although some reusable hydrogel sensors have been investigated,[40] achieving full recycling of hydrogel electronics is difficult. Thus, developing a facile and cost-effective approach to fabricate fully recyclable, stretchable electronic sensors based on naturally occurring hydrogels with a wide operating temperature remains a great challenge.

Herein, we introduced an ionic conductive gelatin organohydrogel with integrated high-strength, antifreezing, and transparent properties for creating green and fully recyclable electronic sensors. The gelatin organohydrogel was easily prepared by immersing the gelatin pre-hydrogel into sodium citrate (Na$_3$Cit) water/glycerol solution. The introduction of a large amount of Na$_3$Cit not only made the organohydrogel exhibit high mechanical performances (*e.g.*, high strength, high stretchability and great fatigue resistance) due to the formation of multiple non-covalent crosslinkings, but also endowed the organohydrogel with excellent conductivity. In addition, the organohydrogel was highly transparent and had a strong anti-freezing capability, even at −60 °C, and the mechanical flexibility and conductivity were well retained. The organohydrogel-based electronic sensor was strain-sensitive with a large linear sensing window and excellent stability. More importantly, our organohydrogel-based sensor can be fully recycled after breaking due to reversible non-covalently crosslinked interactions. As demonstrated, the sensor can be used for accurate human motion detection even at extremely low temperatures.

2. Experimental section

2.1. Materials

All chemicals including gelatin (∼250 Bloom), sodium citrate (Na$_3$Cit) and glycerol were purchased from Aladdin (Shanghai), Inc. Deionized (DI) water was used in the experiments. All the reagents were used as received.

2.2. Preparation of gelatin-based conductive organohydrogels

The gelatin organohydrogel was prepared according to our previous report with minor modifications.[41] Briefly, gelatin solution (10 wt%) was transferred into tubular molds with a diameter of 8.5 mm or rectangular molds with a thickness of 1.0 mm, and then maintained at 4 °C for 30 min to form the gelatin pre-hydrogel. Finally, the gelatin organohydrogel was obtained by soaking the pre-hydrogel into a Na$_3$Cit water/glycerol (1 : 1, w/w) solution mixture with different concentrations (10 wt%, 15 wt%, 20 wt% and 25 wt%) for 3 h. As a control, the gelatin hydrogel was also prepared by soaking the pre-hydrogel into 20 wt% Na$_3$Cit water solution.

2.3. Characterization

Fourier transform infrared spectroscopy (FTIR) spectra were used to monitor the chemical structure of the prepared organohydrogel in the range of 400–4000 cm^{-1} on a Bruker TENSOR 27 FT-IR spectrophotometer. To evaluate the optical transparency of the organohydrogel, the transmittance spectra were obtained by using UV-vis spectroscopy (Thermo EVOLUTION 201) in the visible light range (400–800 nm). The thermal properties of the organohydrogel were investigated using a differential scanning calorimeter (DSC 214, NETZSCH) from 25 to −105 °C at a rate of 2 °C min^{-1}. The rheological test of the organohydrogel was performed using a control-strain rheometer (TA Instruments, New Castle, DE) from 20 to 85 °C with a rate of 2 °C min^{-1} at 1 Hz frequency and 0.1% constant strain.

2.4. Mechanical tests

Tensile and compression tests were performed using a universal electromechanical tester (WDW-05, Si Pai Inc, China) with a 500

4448 | *J. Mater. Chem. A*, 2020, **8**, 4447–4456

This journal is © The Royal Society of Chemistry 2020

N load cell. For both uniaxial and cyclic tensile tests, the organohydrogel specimens with a thickness of *ca.* 0.5 mm were cut into a dumbbell shape (length of 30 mm, width of 2 mm and gauge length of 12 mm) and the stretch rate was fixed at 50 mm min^{-1}. The nominal stress (σ) was obtained by dividing the loading force by the original specimen cross-sectional area, and the nominal strain (ε) was defined as the length change divided by the original length of the samples. The elastic modulus (E) was calculated according to the initial linear slope of the stress–strain curve. The toughness was obtained by integrating the area underneath the stress–strain curve. The dissipated energy (U_{hys}) was estimated from the area below the stress–strain curves. The cylindrical organohydrogel samples with a diameter of 9 mm and height of 6 mm were used for compression tests and the loading rate was fixed at 5 mm min^{-1}.

2.5. Electrical measurements

The conductivity of the organohydrogels was measured by an alternating current impedance method using an electrochemical workstation (Vertex C, IVIUM Tech, Netherlands). During the test, a sinusoidal voltage amplitude of 0.01 V was applied and the frequency range was from 0.01 to 10^5 Hz. The conductivity was determined according to eqn (1):

$$\sigma = \frac{d}{R \times S} \tag{1}$$

where d represents the thickness, R means the resistance and S is the cross-sectional area of the organohydrogel.

For the testing of sensing performances, the tensile strain test was carried out with a universal electromechanical tester, and the relative resistance variations ($\Delta R/R_0$) were recorded with the same electrochemical workstation simultaneously. The strain sensitivity of the organohydrogel was evaluated using the gauge factor (GF), which is defined according to eqn (2):

$$GF = \frac{(R - R_0)/R_0}{\varepsilon} = \frac{\Delta R/R_0}{\varepsilon} \tag{2}$$

where R_0 and R are the resistances of the original and stretched hydrogels, respectively, and ε is the strain applied to the hydrogel.

2.6. Recycling of the gelatin organohydrogel

To recycle the organohydrogel, the fractured organohydrogel fragments were first heated at 70 °C for 30 min to obtain a homogeneous solution. The solution was then transferred into designed molds and placed at 4 °C for 30 min to obtain the recycled organohydrogel. The mechanical, electrical and sensing properties were investigated accordingly.

2.7. Fabrication and testing of the gelatin organohydrogel-based electronic sensor

The organohydrogel (1 mm in thickness) was cut into a strip-shaped specimen with dimensions of 3 cm × 0.8 cm. Afterwards, two copper wires were tightly fixed at the two ends of the organohydrogel specimen to assemble into a flexible strain sensor. VHB tape was used to encapsulate the sensor to minimize the

ambient interference. For detecting human motion, the sensor was attached on different joints of the volunteer directly and the sensing performance was tested using an electrochemical workstation. To demonstrate the sensing performance at subzero temperatures, the sensor was attached to a human model, and the relative resistance variations as the result of motion of the different joints were recorded at −30 °C.

3. Results and discussion

3.1. Design strategy for the gelatin organohydrogel

An antifreezing, high-strength, transparent and conductive gelatin-based organohydrogel was developed *via* constructing multiple non-covalent crosslinking interactions and using a water-glycerol binary solvent as the dispersion medium (Fig. 1). In brief, the gelatin organohydrogel was prepared by simply soaking the gelatin pre-hydrogel, which was crosslinked by triple helix structures as junction zones, in Na_3Cit glycerol/water solution. The exchange of water in the gelatin pre-hydrogel with glycerol in the soaking solution realized transition from the hydrogel to organohydrogel, endowing the organohydrogel with excellent anti-freezing properties. Driven by the concentration difference, plenty of Na^+ and Cit^{3-} would diffuse into the gelatin organohydrogel, resulting in the formation of hydrophobic interchain interaction regions among gelatin chains due to the salting-out effect. Meanwhile, strong ionic interactions can be formed between $-NH_3^+$ of gelatin and Cit^{3-}. The formation of these physically crosslinked domains can greatly enhance the mechanical performances of the organohydrogel. Moreover, this system can obviously reduce the phase separation of the gelatin network owing to the hydrogen bond interactions between glycerol and gelatin, which can effectively improve the transparency of the prepared organohydrogel. In addition, the organohydrogel will be conductive due to the existence of Na^+ and Cit^{3-} ions. More importantly, the fully physically crosslinked structure provided the conditions for the recyclability of the organohydrogel. Finally, the obtained organohydrogel was highly stretchable, conductive, transparent even at extremely low temperatures and fully recyclable.

The synergetic interactions in the organohydrogel were investigated by FTIR. As shown in Fig. S1,† the gelatin pre-hydrogel showed a broad absorption peak at 3280 cm^{-1} for the O–H stretching vibrations and a peak at 1630 cm^{-1} for the amide I bands; the absorption band at 1530 cm^{-1} was attributed to the amide II bands which combine C–N stretching and N–H bending vibrations; the peak at 1391 cm^{-1} was assigned to the C–H bending vibrations and CH_3 symmetrical deformation vibrations. After soaking in Na_3Cit water solution, the intensity of the O–H stretching (3280 cm^{-1}) in the obtained gelatin hydrogel obviously increased, indicating reinforcement of hydrogen bond interactions. Moreover, the intensity of C–H bending vibrations and CH_3 symmetrical deformation vibrations (1391 cm^{-1}) also increased, suggesting that stronger hydrophobic interactions were formed due to the introduction of Na_3Cit.[42] In addition, the absorption band of amide II shifted to higher wavenumbers (1555 cm^{-1}) from 1530 cm^{-1}, suggesting that strong ionic interactions between $-NH_3^+$ and Cit^{3-}

This journal is © The Royal Society of Chemistry 2020

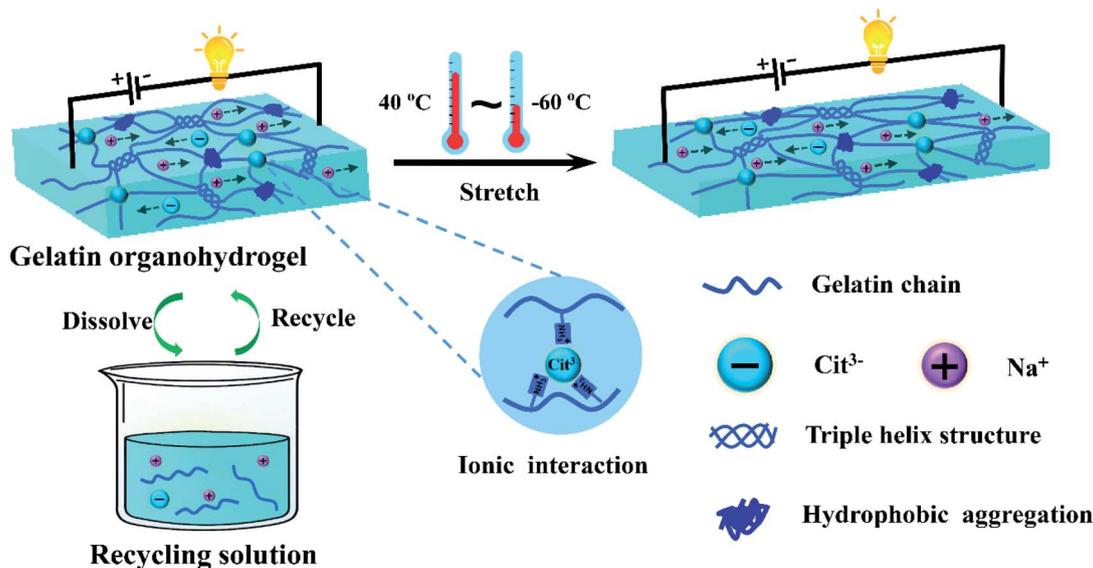*J. Mater. Chem. A*, 2020, **8**, 4447–4456 | **4449**

Fig. 1 Schematic illustration of the structure and versatility of the fully recyclable gelatin organohydrogel. The non-covalent interactions including triple helix structures based on hydrogen bonds, the hydrophobic aggregation induced by the salting-out effect and ionic interactions between the $-NH_3^+$ of gelatin and Cit^{3-} anions are the main driving force for the formation of the organohydrogel. The organohydrogel was transparent, highly stretchable and ionically conductive from 40 to -60 °C.

formed and the conformation of the secondary structure changed.[43,44] For the organohydrogel, except for the above changes, the intensity of the O–H stretching peak was much higher than that of the hydrogel due to the formation of hydrogen bonds between glycerol and gelatin.

3.2. Mechanical properties of the gelatin organohydrogel

To better mimic the functions of human skin and integrate with soft and curvilinear surfaces, high stretchability and

mechanical robustness under repeated movements are required for electronic sensors.[10] The dense network structure originating from the multiple non-covalent interactions can greatly improve the mechanical properties of the organohydrogel. After soaking in Na_3Cit glycerol/water solution, the fragile gelatin pre-hydrogel transformed into a strong gelatin organohydrogel, which could withstand large compression and quickly recover to its original shape when the compression force was removed (Fig. S2†). The obtained organohydrogel could be easily
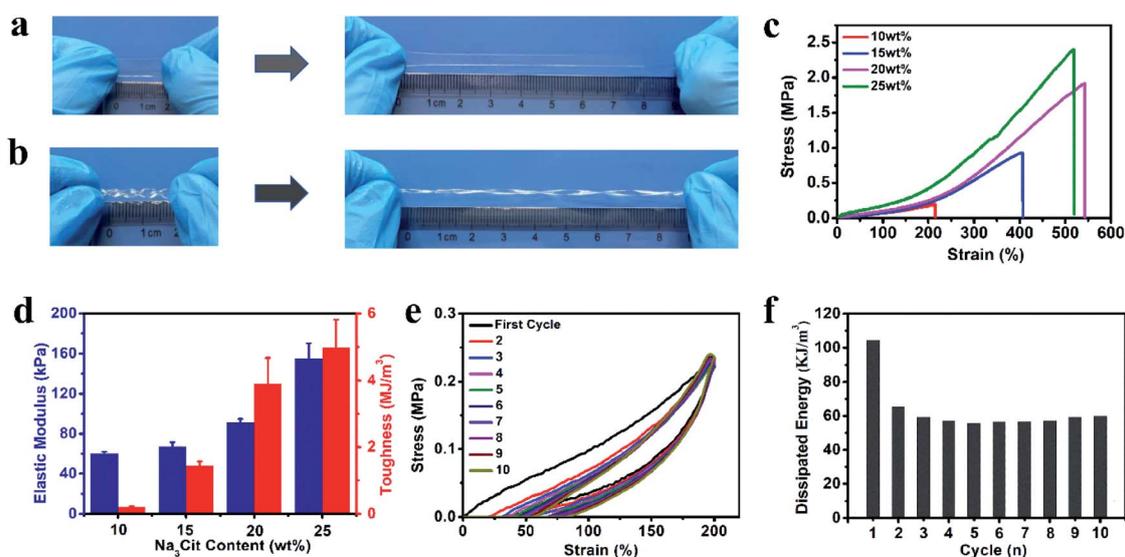

Fig. 2 The mechanical properties of the gelatin organohydrogels. Photographs showing (a) stretching and (b) curly stretching of the gelatin organohydrogels. (c) Tensile curves and (d) the corresponding elastic modulus and toughness of the gelatin organohydrogels soaked in different Na_3Cit concentration solutions. (e) Ten successive cyclic tensile loading–unloading curves and (f) the dissipated energy of the gelatin organohydrogel (20 wt% Na_3Cit).

4450 | *J. Mater. Chem. A*, 2020, **8**, 4447–4456

This journal is © The Royal Society of Chemistry 2020

stretched up to *ca.* 5 times longer than the original length (Fig. 2a) and was flexible enough to withstand the deformation of curly stretching (Fig. 2b), demonstrating high stretchability and superior toughness. The Na$_3$Cit concentration is the main factor to modulate the mechanical performances; as shown in Fig. 2c, the tensile stress and fracture strain dramatically increased from 0.20 MPa and 214% to 1.91 MPa and 542% as the Na$_3$Cit concentration increased from 10 wt% to 20 wt%, respectively. When the Na$_3$Cit concentration further increased to 25 wt%, the tensile stress continued to increase to 2.40 MPa, but the corresponding fracture strain slightly decreased. The remarkable improvement of the mechanical performances of the organohydrogel with the increase of Na$_3$Cit concentration could be due to the changes of the crosslinked network structure. The enhancement of the hydrophobic effect and ionic coordination with the increase of Na$_3$Cit concentration increased the crosslinking density of the gelatin network, improving the rigidity of the organohydrogel network, while the compact crosslinked network structure at a high Na$_3$Cit concentration may deteriorate the ductility.[45] The elastic modulus and toughness exhibited the monotonic variation trend, increasing from 60.0 kPa and 0.21 MJ m^{-3} to 155.0 kPa and 4.99 MJ m^{-3} with the increase of Na$_3$Cit concentration from 10 wt% to 25 wt%, respectively (Fig. 2d).

Considering that the organohydrogel was fully linked by reversible non-covalent interactions, it was expected that the prepared organohydrogel had dissipation and self-recovery ability. As shown in Fig. 2e, a successive cyclic tensile test at a maximum strain of 300% without resting time between each cycle was conducted on the organohydrogel. Apparently, the organohydrogel exhibited a distinct hysteresis loop in the first cycle, indicating that plenty of energy could be dissipated by rapid dissociation of physical interactions in the

organohydrogel network such as hydrophobic association, ionic coordination and hydrogen bonds. From the second to tenth cycles, the hysteresis loops were nearly overlapped with each other, suggesting that the organohydrogel retained the same network structure in the following cycles and exhibited excellent self-recovery ability. The corresponding dissipated energies also remained almost constant during the second to tenth loading cycles (Fig. 2f), confirming the remarkable fatigue resistance of the organohydrogel. In addition, the compression mechanical properties of the organohydrogel were also investigated. As expected, the compression strength and compression modulus greatly improved with the increase of Na$_3$Cit concentration (Fig. S3a and b†). Moreover, the organohydrogel exhibited nearly same hysteresis loops at the cyclic compression tests (Fig. S3c†). These results implied that the prepared organohydrogel had excellent resilience.

3.3. Conductivity of the gelatin organohydrogel in a broad range of temperature

The existence of a large amount of free ions (Na$^+$ and Cit^{3-}) can endow the organohydrogel with excellent conductivity. As shown in Fig. 3a, the conductivity of the organohydrogel was obviously higher that of the pre-hydrogel (0.013 S m^{-1}) and the Na$_3$Cit concentration of the soaking solution had a great influence on the conductivity of the organohydrogels. The conductivity of the organohydrogel gradually increased from 0.29 to 0.47 S m^{-1} when the Na$_3$Cit concentration changed from 10 to 20 wt%. However, when the Na$_3$Cit concentration further increased to 25 wt%, its conductivity decreased to 0.32 S m^{-1}. The conductivity of the organohydrogels could be attributed to two factors: the amount of free ions and the crosslinking density of the organohydrogel.[46] When the Na$_3$Cit concentration increased, more Na$^+$ and Cit^{3-} entered into the organohydrogel,
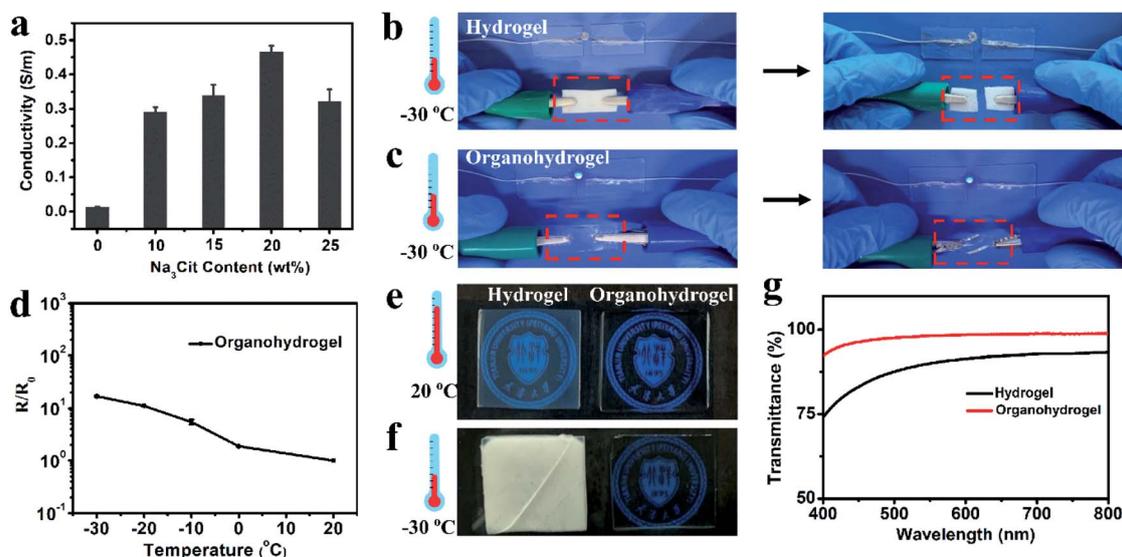

Fig. 3 The conductivity and transparency of the gelatin organohydrogels. (a) The influence of Na$_3$Cit amounts on the conductivity of the organohydrogels. Images showing the conductivity and mechanical robustness of (b) the hydrogel and (c) organohydrogel after freezing at −30 °C for 24 h. (d) R/R_0 of the organohydrogel at different temperatures. Photographs showing the transparency of the hydrogel and organohydrogel at (e) 20 °C and (f) −30 °C. (g) UV-vis transmittance spectra of the hydrogel and organohydrogel at 20 °C.

This journal is © The Royal Society of Chemistry 2020

J. Mater. Chem. A, 2020, **8**, 4447–4456 | **4451**

greatly improving the conductivity. Meanwhile, the crosslinking density of the organohydrogel also increased with the increase of Na_3Cit concentration, and the denser network structure hampered the ionic migration, leading to the decrease of the conductivity. Because of the compromise between the amount of free ions and the crosslinking density, when the Na_3Cit concentration was 20 wt%, the organohydrogel exhibited the best conductivity of 0.47 S m^{-1}.

Traditional conductive hydrogels will be frozen when they are placed at subzero temperatures, and their performances such as mechanical properties and conductivity will further decrease, severely limiting their applications in low-temperature environments.[25] As shown in Fig. 3b, the gelatin hydrogel cannot light up an LED indicator at −30 °C. Moreover, it can be readily frozen to a whitish solid and could be easily broken by bending, indicating that it was unsuitable as an electronic sensor under low temperature conditions. The organohydrogel was flexible enough to withstand twisting at −30 °C due to the anti-freezing properties. According to the DSC curve shown in Fig. S4,† a sharp exothermic peak located at −17.6 °C could be observed in the gelatin hydrogel, while there were no peaks in the whole thermogram from 25 °C to −105 °C for the organohydrogel, further demonstrating the excellent anti-freezing performance. In this non-frozen state, the Na^+ and Cit^{3-} ions in the organohydrogel can still freely migrate, further showing that the organohydrogel maintained excellent conductivity to light an LED indicator at −30 °C, as shown in Fig. 3c; even the organohydrogel was twisted. Actually, the organohydrogel could still maintain conductivity even at −60 °C (Fig. S5a†). The resistance variation of the organohydrogel with the decrease of temperature, as shown in Fig. 3d, indicated that the organohydrogel maintained conductivity well below subzero temperatures and the conductivity of the organohydrogel slightly decreased when the temperature gradually decreased to −30 °C due to the reduction of the migration rate of free ions.[47]

3.4. Transparency of the gelatin organohydrogel in a broad range of temperature

Transparency is an important requirement for electronic sensors that allow visualization of the internal conditions and structures of the devices during the operating process.[27,29,48] The hydrogen bonds between the gelatin and glycerol impeded the phase separation of the gelatin network, making the organohydrogel highly transparent. As shown in Fig. 3e, the university logos under both the gelatin hydrogel and organohydrogel could be seen, but the logo behind the organohydrogel was clearer compared with that behind the hydrogel. The transparency was further investigated by testing their transmittance in the wavelength range of 400–800 nm. From Fig. 3g, it could be seen that the average optical transmittance of the organohydrogel could reach 96%, demonstrating the ultrahigh transparency. The hydrogel showed very poor transparency at low temperature due to the formation of ice crystals. The gelatin hydrogel was frozen and became a white solid. Our previous study suggested that the organohydrogel had excellent antifreezing properties because glycerol can form plenty of strong hydrogen bond clusters with water and inhibit freezing of the remaining water in organohydrogel networks. Thus, the organohydrogel was not frozen and still maintained high transparency even at −30 and −60 °C (Fig. 3f and S5b†). To highlight the advantages of the organohydrogel designed in our work as a green, transparent and stretchable electronic sensor, a systematic comparison of our organohydrogel with previously reported natural polymer-based hydrogels is shown in Table S1.† It could be clearly seen that our organohydrogel possessed the best integration of tensile strength, stretchability, conformability, high conductivity and transparency, indicating its promising applications as a green and flexible electronic device.
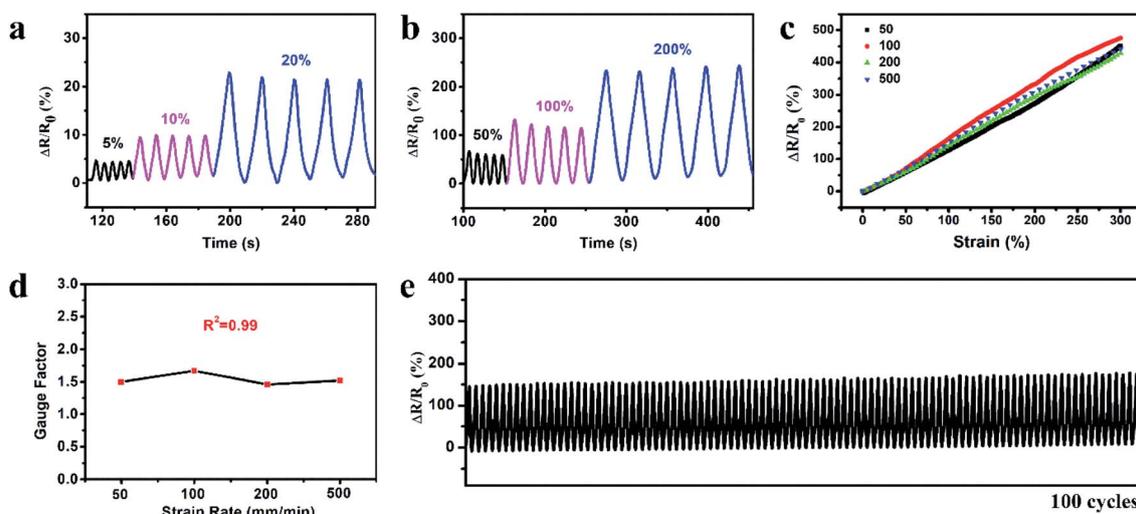

Fig. 4 The electromechanical characterization of the organohydrogel-based electronic sensor. Relative resistance changes ($\Delta R/R_0$) at different cyclic stretching−releasing levels: (a) small strains (5, 10 and 20%) and (b) large strains (50, 100 and 200%). (c) $\Delta R/R_0$ *versus* the applied strains up to 300% at different displacement rates (50, 100, 200 and 500 mm min^{-1}) and (d) the corresponding gauge factors. (e) The durability test under repeated strains of 100% for 100 cycles.

4452 | *J. Mater. Chem. A*, 2020, **8**, 4447–4456

This journal is © The Royal Society of Chemistry 2020

3.5. Gelatin organohydrogel-based electronic sensor

The organohydrogel was exploited to fabricate the strain sensor and the strain sensing performance was investigated. Fig. 4a and b show the relative resistance variation ($\Delta R/R_0$) of the organohydrogel at small strains (5, 10 and 20%) and large strains (50, 100 and 200%) during five cycles of the stretching–releasing process. The response signals were distinctly different for different strains and the patterns of each cycle were highly similar at the same strain, indicating that the organohydrogel could be able to detect and differentiate various levels of strains with excellent reliability. The reliable sensing performance is also illustrated in Movie S1;† an LED indicator in the circuit displayed alternate luminance variation during stretching and releasing the organohydrogel. To investigate the resistance variation with the gradual changes of the strain, we stretched the organohydrogel to 300% at different displacement rates, and recorded the corresponding resistance signals. Fig. 4c shows a typical plot of $\Delta R/R_0$ versus strains at four displacement rates of 50, 100, 200 and 500 mm min^{-1}. It could be clearly seen that the $\Delta R/R_0$ of the organohydrogel-based sensor exhibited a linear increase in the whole strain region of 0–300%, and response signals were nearly consistent for the displacement rate from 50 to 500 mm min^{-1}. The strain sensitivity was evaluated using the gauge factor (GF) according to eqn (2) with the linear fitting curves in Fig. 4c. Fig. 4d shows that the GF was ca.

1.5 in the 0–300% strain range at different displacement rates, implying that the strain sensor possessed high sensitivity without any dependency on the displacement rates. The linear response and high sensitivity without rate-dependence could be attributed to the uniform deformation of the network upon stretching and high elasticity of the organohydrogel.[49] In addition, the response rate of the organohydrogel was investigated, with the response time when loading and relaxation time when unloading being 200 ms and 400 ms (Fig. S6†), respectively, indicating a fast strain response, which could ensure the real-time sensing for various motions. Stability and durability are greatly important for applications of strain sensors. To evaluate the stability of the strain sensor, 100 cycles of stretching and releasing at 100% strain was conducted. As shown in Fig. 4e, the $\Delta R/R_0$ exhibited good repeatability and negligible fluctuation over the entire durability test. Furthermore, the rheological behaviors and durability test of the organohydrogel indicated that the organohydrogel-based strain sensor was stable when the temperature was below 40 °C (Fig. S7 and S8†).

3.6. Recyclability of the gelatin organohydrogel-based electronic sensor

For most previously reported electronic sensors, the rupture of materials would cause the function failure of electronic devices, producing a mass of electronic waste and increasing the
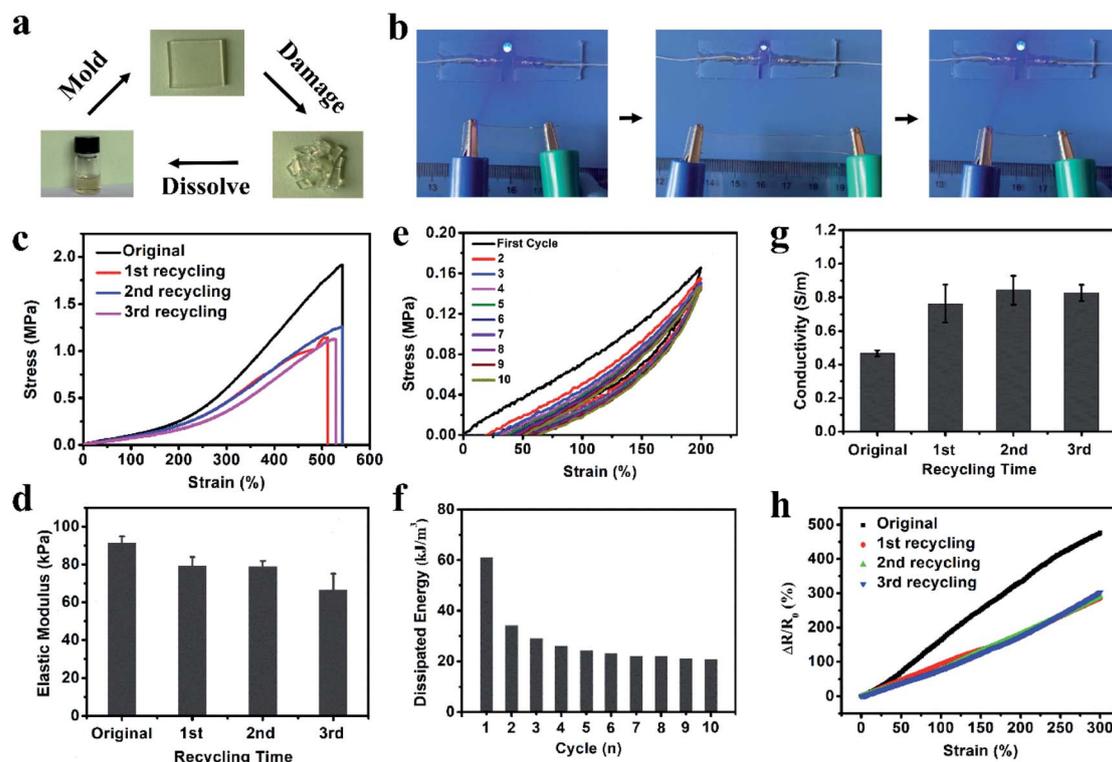

Fig. 5 Recyclability of the gelatin organohydrogel. (a) Demonstration of the recycling process. When mechanically broken, the organohydrogel can be recycled by fusing the organohydrogel fragments at 70 °C and remolding at 4 °C. (b) Images showing that the recycled organohydrogel was highly stretchable and ionically conductive under large deformation. (c) Tensile stress–strain curves and (d) the corresponding elastic modulus of the organohydrogel before and after recycling. (e) Successive loading–unloading curves and (f) the dissipated energies of the recycled organohydrogel. (g) Conductivity and (h) $\Delta R/R_0$ as a function of strains up to 300% of the organohydrogel before and after recycling.

manufacturing cost.[39,50] The reusable electronics may provide great potential for solving this problem. Our organohydrogel was fully crosslinked by non-covalent interactions including hydrogen bonds, ionic bonds and hydrophobic association. These reversible interactions can endow the organohydrogel with good recyclability. As a proof-of-concept, the organohydrogel was cut into fragments to mimic the break of the sensor by the external force; then, these organohydrogel fragments were fully transformed into a homogeneous sol state after being incubated at 70 °C for 20 min. When stored at 4 °C for 10 min, the sol turned into a gel state again and a new organohydrogel formed, achieving full recyclability (Fig. 5a). The recycling process could be completed within 1 hour, exhibiting a rapid manufacturing process.

The reused organohydrogel could almost recover its original performances and functions. As shown in Fig. 5b, the recycled organohydrogel was still mechanically tough to sustain the large deformation of stretching and had high resilience to recover to its original size when the stretching was released. Meanwhile, the LED indicator was lit when the recycled organohydrogel was connected in a circuit. As the same with the original organohydrogel, the luminance of the LED indicator varied periodically upon stretching and releasing the organohydrogel. These results indicated that the recycled organohydrogel was conductive and strain-sensitive. To further

demonstrate the usability, the mechanical and electrochemical tests were conducted on the organohydrogel after recycling up to three times. Fig. 5c and d show the tensile stress–strain curves and corresponding elastic modulus of the organohydrogel before and after recycling three times, respectively. It could be observed that the recycled organohydrogel had a high tensile strain of *ca.* 500%. The tensile strength of the recycled organohydrogel surpassed 1 MPa, although it decreased compared with the original organohydrogel. It should be noted that the elastic modulus exhibited only a slight decrease. In addition, a successive cyclic tensile test and the corresponding dissipated energies indicated that the recycled organohydrogel also had remarkable fatigue resistance (Fig. 5e and f). The recycled organohydrogel was highly transparent as the original one (Fig. S9†). Interestingly, the conductivity of the recycled organohydrogel increased compared with that of the organohydrogel (Fig. 5g). The decrease of mechanical performances and the increase of conductivity might be attributed to the reduction of non-covalent interactions such as ionic bonds, resulting in the decrease of cross-linking density and the increase of free ions. More importantly, the recycled organohydrogel-based strain sensor also possessed high sensitivity (Fig. 5h). These results demonstrated that the organohydrogel can be reused for the fabrication of electronic sensors. Furthermore, as shown in Table S2,† although other types of
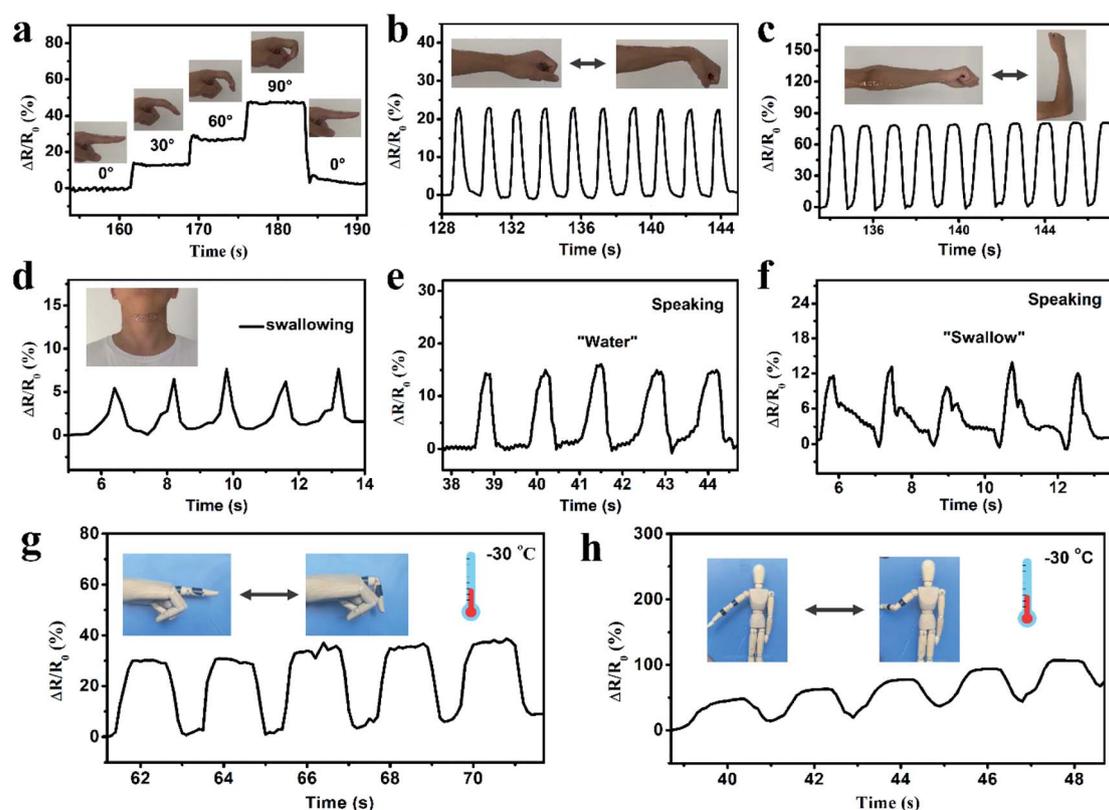

Fig. 6 Demonstration of sensing applications of a wearable organohydrogel-based electronic sensor. $\Delta R/R_0$ of (a) finger bending at various angles, (b) elbow rotation and (c) wrist bending. Detection of subtle motions of (d) swallowing and pronouncing different words: (e) ″water″ and (f) ″swallow″. The wearable electronic sensor attached to (g) a prosthetic finger for monitoring finger bending and (h) human model for detecting elbow rotation at −30 °C.

4454 | *J. Mater. Chem. A*, 2020, **8**, 4447–4456

This journal is © The Royal Society of Chemistry 2020

conductive gel-based electronics showed some functionalities such as stretchability, anti-freezing properties and transparency,[28,29,32,40,51,52] the green, fully recyclable and stretchable electronic sensors with ultra-low operating temperature developed in our work are hardly achieved in these reported electronics.

3.7. Applications of the gelatin organohydrogel-based electronic sensor

In order to investigate the applications of the prepared organohydrogels in wearable sensors, an organohydrogel-based strain sensor was used to monitor full-range human activities in real time. First, the strain sensor was assembled on human joints (finger, elbow, wrist, and knee joints) to detect the joint motions. As shown in Fig. 6a, when the finger was bent stepwise from the straightened state to 30°, 60° and 90°, the $\Delta R/R_0$ gradually increased to 12, 27, and 47%, respectively. The $\Delta R/R_0$ at the same bending angle remained constant and the resistance value immediately returned to its original levels when the finger was straightened. The strain sensor can also be used to precisely monitor the extending/flexing of the elbow, as shown in Fig. 6b; the response signals were repeatable and stable during the cyclic extending/flexing process. Similarly, other joint motions such as knee and wrist bending could also be detected by the strain sensor with great stability and repeatability (Fig. 6c and S10†). In addition to large human motions, the monitoring of subtle physiological motions could be achieved using the organohydrogel-based strain sensor. As shown in Fig. 6d, the strain sensor was attached to the throat of a male volunteer to monitor the movement by swallowing motions. The resistance signals were obvious and relatively consistent when the volunteer performed periodic swallowing motions. Furthermore, the organohydrogel-based strain sensor could be also used to detect and distinguish pronouncing. The resistance patterns were similar when the tester pronounced the same word repeatedly, while the strain sensor showed distinguishable resistance signals when saying different words, such as "water" and "swallow" (Fig. 6e and f). More importantly, the organohydrogel-based strain sensor could also operate at extremely low temperatures due to the antifreezing properties. When the organohydrogel was attached to a human model, the finger and elbow bending at −30 °C could be detected with good repeatability (Fig. 6g and h). All these results demonstrate that the organohydrogel-based electronic sensor has great potential as a wearable device to detect full-range human activities in wide temperature ranges.

4. Conclusion

In summary, we have presented the successful fabrication of a fully recyclable and stretchable electronic sensor with wide ultra-low operating temperature from a high-strength, highly transparent and antifreezing gelatin organohydrogel. This organohydrogel was prepared by simply treating the gelatin prehydrogel with citrate (Na$_3$Cit) water/glycerol solution. The obtained organohydrogel showed high tensile strength, large elongation and excellent ionic conductivity due to generation of multiple supramolecular interactions induced by Na$_3$Cit and the existence of a large amount of free salt ions. Moreover, the water–glycerol binary solvent as the dispersion medium endowed the organohydrogel with high transparency and excellent antifreezing properties, and the mechanical flexibility and ionic conductivity could be retained even at −60 °C. The electronic sensor based on this organohydrogel was strain-sensitive with a large linear sensing window and excellent stability. More importantly, the organohydrogel electronic sensor could be fully recycled because of reversible non-covalently crosslinked interactions. The recycled organohydrogel electronic sensor exhibited good mechanical and electrical properties and strain sensing performances. Furthermore, this organohydrogel electronic sensor could be used to monitor full-range human activities even at extremely low temperatures. This transparent, green, recyclable and stretchable organohydrogel electronic sensor with a broad operating temperature range will find wide applications in electronic skins, health monitoring and biomedical devices.

Conflicts of interest

There are no conflicts to declare.

Acknowledgements

Notes and references

1 D. Son, J. Lee, S. Qiao, R. Ghaffari, J. Kim, J. E. Lee, C. Song, S. J. Kim, D. J. Lee, S. W. Jun, S. Yang, M. Park, J. Shin, K. Do, M. Lee, K. Kang, C. S. Hwang, N. Lu, T. Hyeon and D. H. Kim, *Nat. Nanotechnol.*, 2014, **9**, 397–404.

2 S. Xu, Y. Zhang, L. Jia, K. E. Mathewson, K. I. Jang, J. Kim, H. Fu, X. Huang, P. Chava, R. Wang, S. Bhole, L. Wang, Y. J. Na, Y. Guan, M. Flavin, Z. Han, Y. Huang and J. A. Rogers, *Science*, 2014, **344**, 70–74.

3 M. K. Choi, J. Yang, D. C. Kim, Z. Dai, J. Kim, H. Seung, V. S. Kale, S. J. Sung, C. R. Park, N. Lu, T. Hyeon and D. H. Kim, *Adv. Mater.*, 2018, **30**, 1703279.

4 S. Park, S. W. Heo, W. Lee, D. Inoue, Z. Jiang, K. Yu, H. Jinno, D. Hashizume, M. Sekino, T. Yokota, K. Fukuda, K. Tajima and T. Someya, *Nature*, 2018, **561**, 516–521.

5 Y. Ma, Y. Zhang, S. Cai, Z. Han, X. Liu, F. Wang, Y. Cao, Z. Wang, H. Li, Y. Chen and X. Feng, *Adv. Mater.*, 2019, 1902062.

6 J. Kim, H. J. Shim, J. Yang, M. K. Choi, D. C. Kim, J. Kim, T. Hyeon and D. H. Kim, *Adv. Mater.*, 2017, **29**, 1606134.

7 B. C. K. Tee, A. Chortos, A. Berndt, A. K. Nguyen, A. Tom, A. McGuire, Z. C. Lin, K. Tien, W. G. Bae, H. Wang, P. Mei,

This journal is © The Royal Society of Chemistry 2020

J. Mater. Chem. A, 2020, **8**, 4447–4456 | **4455**

H. H. Chou, B. Cui, K. Deisseroth, T. N. Ng and Z. Bao, *Science*, 2015, **350**, 313–316.

8 C. Wang, K. Xia, Y. Zhang and D. L. Kaplan, *Acc. Chem. Res.*, 2019, **52**, 2916–2927.

9 X. Wang, X. Lu, B. Liu, D. Chen, Y. Tong and G. Shen, *Adv. Mater.*, 2014, **26**, 4763–4782.

10 S. Yao, P. Ren, R. Song, Y. Liu, Q. Huang, J. Dong, B. T. O'Connor and Y. Zhu, *Adv. Mater.*, 2019, 1902343.

11 J. Y. Sun, C. Keplinger, G. M. Whitesides and Z. Suo, *Adv. Mater.*, 2014, **26**, 7608–7614.

12 S. Lin, H. Yuk, T. Zhang, G. A. Parada, H. Koo, C. Yu and X. Zhao, *Adv. Mater.*, 2016, **28**, 4497–4505.

13 Z. Wang, H. Zhou, J. Lai, B. Yan, H. Liu, X. Jin, A. Ma, G. Zhang, W. Zhao and W. Chen, *J. Mater. Chem. C*, 2018, **6**, 9200–9207.

14 J. Wu, Z. Wu, H. Xu, Q. Wu, C. Liu, B. R. Yang, X. Gui, X. Xie, K. Tao, Y. Shen, J. Miao and L. K. Norford, *Mater. Horiz.*, 2019, **6**, 595–603.

15 D. Men, F. Zhou, L. Hang, X. Li, G. Duan, W. Cai and Y. Li, *J. Mater. Chem. C*, 2016, **4**, 2117–2122.

16 D. Men, H. Zhang, L. Hang, D. Liu, X. Li, W. Cai, Q. Xiong and Y. Li, *J. Mater. Chem. C*, 2015, **3**, 3659–3665.

17 J. Wu, S. Han, T. Yang, Z. Li, Z. Wu, X. Gui, K. Tao, J. Miao, L. K. Norford, C. Liu and F. Huo, *ACS Appl. Mater. Interfaces*, 2018, **10**, 19097–19105.

18 G. Cai, J. Wang, K. Qian, J. Chen, S. Li and P. S. Lee, *Adv. Sci.*, 2017, **4**, 1600190.

19 J. Duan, X. Liang, J. Guo, K. Zhu and L. Zhang, *Adv. Mater.*, 2016, **28**, 8037–8044.

20 Q. Liu, M. Zhang, L. Huang, Y. Li, J. Chen, C. Li and G. Shi, *ACS Nano*, 2015, **9**, 12320–12326.

21 X. Sun, Z. Qin, L. Ye, H. Zhang, Q. Yu, X. Wu, J. Li and F. Yao, *Chem. Eng. J.*, 2020, **382**, 122832.

22 H. Gao, Z. Zhao, Y. Cai, J. Zhou, W. Hua, L. Chen, L. Wang, J. Zhang, D. Han, M. Liu and L. Jiang, *Nat. Commun.*, 2017, **8**, 15911.

23 D. C. Kim, H. J. Shim, W. Lee, J. H. Koo and D. Kim, *Adv. Mater.*, 2019, 1902743.

24 L. Han, L. Yan, M. Wang, K. Wang, L. Fang, J. Zhou, J. Fang, F. Ren and X. Lu, *Chem. Mater.*, 2018, **30**, 5561–5572.

25 Q. Rong, W. Lei, L. Chen, Y. Yin, J. Zhou and M. Liu, *Angew. Chem., Int. Ed.*, 2017, **56**, 14159–14163.

26 C. Yang and Z. Suo, *Nat. Rev. Mater.*, 2018, **3**, 125–142.

27 C. C. Kim, H. H. Lee, K. H. Oh and J. Y. Sun, *Science*, 2016, **353**, 682–687.

28 X. Zhang, N. Sheng, L. Wang, Y. Tan, C. Liu, Y. Xia, Z. Nie and K. Sui, *Mater. Horiz.*, 2019, **6**, 326–333.

29 X. Pan, Q. Wang, R. Guo, Y. Ni, K. Liu, X. Ouyang, L. Chen, L. Huang, S. Cao and M. Xie, *J. Mater. Chem. A*, 2019, **7**, 4525–4535.

30 Y. Yang, L. Guan, X. Li, Z. Gao, X. Ren and G. Gao, *ACS Appl. Mater. Interfaces*, 2019, **11**, 3428–3437.

31 X. P. Morelle, W. R. Illeperuma, K. Tian, R. Bai, Z. Suo and J. J. Vlassak, *Adv. Mater.*, 2018, **30**, 1801541.

32 Y. Xia, Y. Wu, T. Yu, S. Xue, M. Guo, J. Li and Z. Li, *ACS Appl. Mater. Interfaces*, 2019, **11**, 21117–22112.

33 J. Wu, Z. Wu, S. Han, B. R. Yang, X. Gui, K. Tao, C. Liu, J. Miao and L. K. Norford, *ACS Appl. Mater. Interfaces*, 2018, **11**, 2364–2373.

34 Y. H. Jung, T. H. Chang, H. Zhang, C. Yao, Q. Zheng, V. W. Yang, H. Mi, M. Kim, S. J. Cho, D. W. Park, H. Jiang, J. Lee, Y. Qiu, W. Zhou, Z. Cai, S. Gong and Z. Ma, *Nat. Commun.*, 2015, **6**, 7170.

35 L. Wang, D. Chen, K. Jiang and G. Shen, *Chem. Soc. Rev.*, 2017, **46**, 6764–6815.

36 R. Tong, G. Chen, D. Pan, H. Qi, R. Li, J. Tian, F. Lu and M. He, *Biomacromolecules*, 2019, **20**, 2096–2104.

37 M. Jo, K. Min, B. Roy, S. Kim, S. Lee, J. Y. Park and S. Kim, *ACS Nano*, 2018, **12**, 5637–5645.

38 M. M. Pakulska, K. Vulic, R. Y. Tam and M. S. Shoichet, *Adv. Mater.*, 2015, **27**, 5002–5008.

39 L. Teng, S. Ye, S. Handschuh-Wang, X. Zhou, T. Gan and X. Zhou, *Adv. Funct. Mater.*, 2019, **29**, 1808739.

40 H. Liu, M. Li, C. Ouyang, T. J. Lu, F. Li and F. Xu, *Small*, 2018, **14**, 1801711.

41 Z. Qin, D. Dong, M. Yao, Q. Yu, X. Sun, Q. Guo, H. Zhang, F. Yao and J. Li, *ACS Appl. Mater. Interfaces*, 2019, **11**, 21184–21193.

42 D. Chandler, *Nature*, 2005, **437**, 640–647.

43 Q. Chang, M. A. Darabi, Y. Liu, Y. He, W. Zhong, K. Mequanin, B. Li, F. Lu and M. M. Q. Xing, *J. Mater. Chem. A*, 2019, **7**, 24626–24640.

44 Q. He, Y. Huang and S. Wang, *Adv. Funct. Mater.*, 2018, **28**, 1705069.

45 Y. Yang, X. Wang, F. Yang, L. Wang and D. Wu, *Adv. Mater.*, 2018, **30**, 1707071.

46 Z. Tang, X. Lyu, A. Xiao, Z. Shen and X. Fan, *Chem. Mater.*, 2018, **30**, 7752–7759.

47 D. Lou, C. Wang, Z. He, X. Sun, J. Luo and J. Li, *Chem. Commun.*, 2019, **55**, 8422–8425.

48 T. Li, Y. Li and T. Zhang, *Acc. Chem. Res.*, 2019, **52**, 288–296.

49 S. Xu, D. M. Vogt, W. H. Hsu, J. Osborne, T. Walsh, J. R. Foster, S. K. Sullivan, V. C. Smith, A. W. Rousing, E. C. Goldfield and R. J. Wood, *Adv. Funct. Mater.*, 2019, **29**, 1807058.

50 B. H. Robinson, *Sci. Total Environ.*, 2009, **408**, 183–191.

51 J. Wu, Z. Wu, X. Lu, S. Han, B. Yang, X. Gui, K. Tao, J. Miao and C. Liu, *ACS Appl. Mater. Interfaces*, 2019, **11**, 9405–9414.

52 G. Ge, Y. Zhang, J. Shao, W. Wang, W. Si, W. Huang and X. Dong, *Adv. Funct. Mater.*, 2019, **28**, 1802576.